UC Irvine
UC Irvine Previously Published Works

Title

Anatomic optical coherence tomography of upper airways

Permalink

ISBN

Authors

Loy, AC
Jing, J
Zhang, J
et al.

Publication Date

2015

DOI

Copyright Information

Peer reviewed

Anatomic Optical Coherence Tomography of Upper Airways

Anthony Chin Loy, Joseph Jing, Jun Zhang, Yong Wang,
Said Elghobashi, Zhongping Chen, and Brian J. F. Wong

75.1 Introduction

The upper airway is a complex and intricate system responsible for respiration, phonation, and deglutition. Obstruction of the upper airways, as in obstructive sleep apnea (OSA), afflicts 12–18 million Americans. Pharyngeal size and shape are important factors in the pathogenesis of OSA. Nocturnal loss in pharyngeal muscular tone combined with high pharyngeal resistance leads to collapse of the airway and periodic partial or complete upper airway obstruction. These episodes, though brief, can lead to significant adverse health outcomes, including cardiac,

A. Chin Loy
Department of Otolaryngology Head and Neck Surgery, The Beckman Laser Institute, University of California Irvine, Irvine, CA, USA

J. Jing • J. Zhang
Department of Biomedical Engineering, The Beckman Laser Institute, University of California Irvine, Irvine, CA, USA

Y. Wang • S. Elghobashi
Department of Mechanical and Aerospace Engineering, University of California Irvine, Irvine, CA, USA

Z. Chen (✉)
The Edwards Life Sciences Center for Advanced Cardiovascular Technology, Beckman Laser Institute, Irvine, CA, USA

Department of Biomedical Engineering, Beckman Laser Institute, University of California Irvine, Irvine, CA, USA
e-mail: z2chen@uci.edu

B.J.F. Wong (✉)
Department of Otolaryngology Head and Neck Surgery, Department of Biomedical Engineering, Department of Surgery, The Beckman Laser Institute, University of California Irvine, Irvine, CA, USA
e-mail: bjwong@uci.edu

neurologic, and metabolic sequelae. Though prevalent in the population, the pathogenesis of OSA is poorly understood. The most common explanation in the literature assumes that OSA is a function of decreased pharyngeal size with concomitant increased pharyngeal resistance. These factors combined with the relaxation of the pharyngeal dilator muscles predispose the pharynx to collapse during sleep.

The three major areas of obstruction are the nose, the palate, and the hypopharynx though it is more likely the combination of two or more of these areas that contribute to OSA. In the Fujita classification, the patterns of obstruction were classified by anatomic location:

1. Type 1: collapse in the retropalatal region only
2. Type 2: collapse in both the retropalatal and retrolingual regions
3. Type 3: collapse in the retrolingual region only

The identification of the area of collapse is needed to direct surgical treatment though this is not often accomplished, and clinical judgment largely dictates the selection of operative approach. Operations and procedures are directed at the most common areas of obstruction. Nasal surgery includes septoplasty, turbinate reduction, and correction of internal and external valve deformities. Nasal surgery rarely corrects OSA by itself, but does allow greater nasal patency for use of Continuous Positive Airway Pressure (CPAP). The most common operation used to treat OSA is the uvulopalatopharyngoplasty (UPPP), which is performed by resecting redundant palatal and pharyngeal tissue. Though it is the most common operation for OSA, the procedure has a widely cited success rate of less than 50 % depending on the severity of disease [1]. Other OSA operations escalate in complexity and address other organs and tissue, but lack of detailed anatomic information on the site or level of obstruction leads to modest improvement in a majority of patients. More aggressive procedures include base of tongue reduction, advancement of the maxilla and mandible to anteriorly displace the base of tongue, suspension of the larynx to the chin, and even tracheostomy.

The failure rate in the surgical treatment OSA stems from a lack of diagnostic information on the site and mechanism of airway collapse. Current diagnostic techniques include magnetic resonance imaging (MRI) and computed tomography (CT), though these studies are not routinely ordered, as MRI and CT are expensive, inconvenient for the patient, generally performed during wakefulness, and in the case of CT necessitate exposure to ionizing radiation. MRI provides great detail of the soft tissue structures of the upper airways while avoiding exposure to ionizing radiation. However, the study is expensive, while the length and noise of the exam may prevent collection of sleep data without sedation. Use of sedatives alters normal physiological control of the pharyngeal musculature and hence limits the utility of this approach in mimicking natural sleep. In regard to young children, sedation is necessary to perform MRI. Computed tomography provides detailed images of bone and soft tissue and is a considerably shorter exam than MRI. However, the exposure to ionizing radiation limits serial examinations over the respiratory cycle, limits the use of multiple exams to document postoperative

changes, and again is applied conservatively in children. Both MRI and CT provide information at a single point in time; they fail to provide volumetric data over the course of the breathing cycle.

More frequently, in-office fiber-optic endoscopy is used to estimate the loci for pharyngeal collapse in the OSA patient. Use of the Mueller maneuver, inhalation against a closed nose and mouth, to identify areas of obstruction is commonly used to better identify surgical treatment targets. The image of the airway through an endoscope is subject to significant distortion due to the wide-angle optics of these instruments. Measurements of airway diameter are thus largely subjective and are dependent on the relative location of the endoscope within the airway [2].

Polysomnography remains the gold standard in the diagnosis of OSA. Polysomnography (e.g., sleep study) is a multiparametric test used in the study of sleep and as a diagnostic tool in sleep medicine. It is an overnight diagnostic test performed during natural sleep that includes electroencephalography; electrooculography; measurement of nasal and oral airflow; electromyography, body, chest, and abdomen position monitors; electrocardiography; and pulse oximetry. Though extensive, it provides only physiological data for diagnosis; it does not provide structural data for treatment [1]. In face of the limitations of current clinically available methods to diagnose OSA, multiple alternative technologies have been proposed as a means to identify the locus of airway obstruction. Sampson's group in Perth developed a long-range optical coherence tomography (LR-OCT) system as a minimally invasive and cost-effective means of acquiring detailed structural data of the upper airway [3, 4]. It is safe for use in patients requiring multiple scans as no ionizing radiation is involved. It allows the physician to acquire serial data sets for the analysis of pre- and postoperative states. The lack of ionizing radiation also makes it safe for extended exposure, and the use of contemporary Fourier-domain technology facilitates rapid data collection with the entire length of an airway scanned in less than 1 min. In LR-OCT, a very small diameter catheter (smaller than conventional endoscopes) is inserted through the nose and into the pharynx. The placement of this imaging probe is similar to the placement of a feeding tube, pH monitor, or fiber-optic endoscope – all of which are routinely placed by physicians in multiple specialties. The probe tip rotates thus acquiring axial images of the pharynx, which can be reconstructed to evolve a structural image of the airway. In this implementation, the technology functions as an optical range finder, and high-resolution anatomic information of the subsurface tissues is not required. LR-OCT provides detailed structural and quantitative data of the upper airway that is not provided by current diagnostic imaging [5]. This information is crucial to the advancement of understanding the pathophysiology of OSA and the application of treatment to specific problem areas of the airway.

Conventional OCT provides detailed three-dimensional tomographic images of tissues with high axial and lateral resolution and beyond ophthalmology has found several uses in the imaging of hollow organs such as the urinary [6], GI [7], and pulmonary systems [8–12] However, the conventional use of OCT in the upper airways for structural imaging is limited due to a scanning range of only a few

millimeters or less. Long-range optical coherence tomography (LR-OCT) works as an optical range finder in circumstances where detailed microanatomic information on the surface is not required. Rather than focusing on microscopic substructure, LR-OCT increases the axial scanning range to image macroscopic anatomy [13]. This application is well suited for imaging the upper airway, where gross images can be used to examine the contours of the airway.

Long-range OCT systems were first described by Leitgeb, who used a phase shifting algorithm in order to double the effective imaging range of conventional OCT. With the increased imaging distance, the system used by Leitgeb also utilized frequency-domain optical coherence tomography to achieve high-speed probing [14]. In Sampson's group the use of LR-OCT in the upper airway is first mentioned in 2003 to measure the area of the human pharynx in patients with sleep apnea. The LR-OCT used at that time had a radial scanning range of 26 mm and a rotation rate of 5 Hz [15]. When first demonstrated by Huang in 1991, OCT was primarily used in ophthalmic imaging. Compared to the systems being used today, OCT was dominated by time-domain imaging. Time-domain imaging is limited by the need to scan through various path lengths in the reference arm in order for the sample arm to be interpreted. In the dynamic upper airway, slow scanning speeds produce motion artifact during the respiratory cycle [16]. In 1995, Fercher described Fourier-domain OCT (FD-OCT), which allowed for high-speed image acquisition (up to 100 times) and a decreased signal-to-noise ratio when compared with time-domain OCT [17]. FD-OCT measures all the optical echoes at once rather than sequentially as in time-domain OCT. This significantly increases sensitivity. Mechanical scanning of the reference path is unnecessary in FD-OCT, increasing the axial scan rate and imaging speed [18]. In recent studies utilizing a time-domain system, a lengthwise scan of the upper airway (12–18 cm) is completed in 12 min [19]. In the following, we describe an LR-OCT system using Fourier domain that is capable of completing a scan of comparable distance of the human airway in under a minute. The increased speed of acquisition decreases motion artifact experienced in previous experiments and negates the need to use respiratory gating to account for changes in the diameter of the airway that would be experienced in slower systems. There has been an increased level of interest in FD-OCT since then with developments improving the quality and speed of the systems. Recent systems employing Fourier-domain locked lasers have shown imaging speeds up to 370,000 axial scans/s, 100 times faster than standard OCT [20].

75.2   Current System

The current system is a catheter-based Fourier-domain optical coherence tomography (Fig. 75.1). Output light from a 1,310-nm swept source laser (26-mW average power, 50-kHz A-scan rate, 102-nm FWHM bandwidth, 5-mm coherence length in air) is split by a 90–10 couple into sample and reference arms, respectively. The reference arm utilizes an acousto-optic modulator (AOM) to generate a carrier
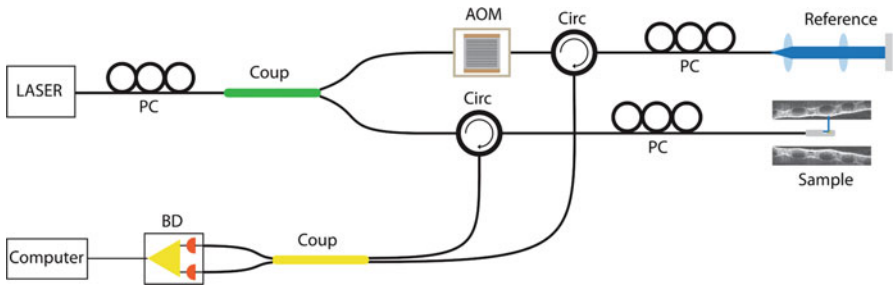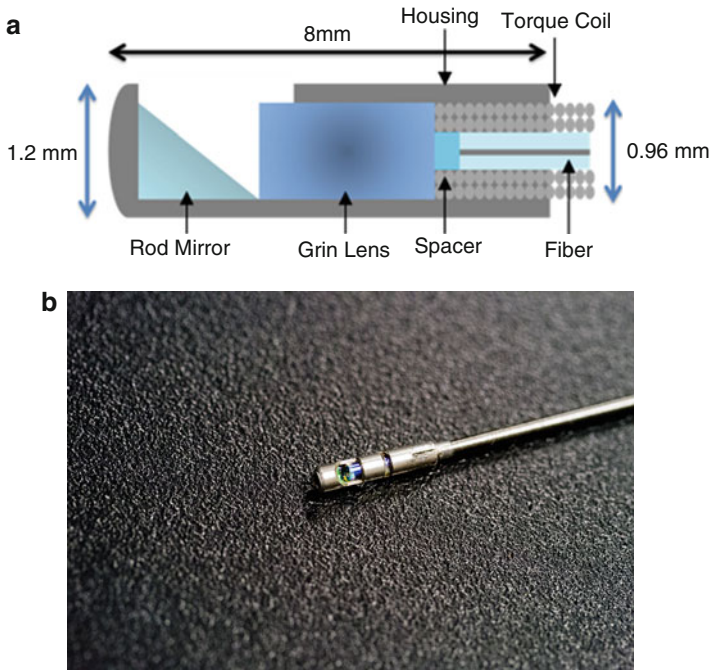
Fig. 75.1 Current long-range OCT system

Fig. 75.2 Schematic (**a**) and picture (**b**) of LR-OCT probe

frequency of 150 MHz. No modulator is used in the sample arm to maximize signal and prevent insertion loss typically seen in AOMs. The resulting signal is converted in a voltage signal by a balanced detector and sampled by a 12-bit data acquisition card. Digitizing is performed at a sampling rate of 1 GHz allowing complete coverage of the wavelength sweep in 8192 points to optimize subsequent fast Fourier transform (FFT) calculations. The endoscopic OCT probe (Fig. 75.2) has an outer diameter (OD) of 1.2 mm, smaller than conventional endoscopes currently used in clinics. Rotational scanning is accomplished by using a fiber-optic rotary
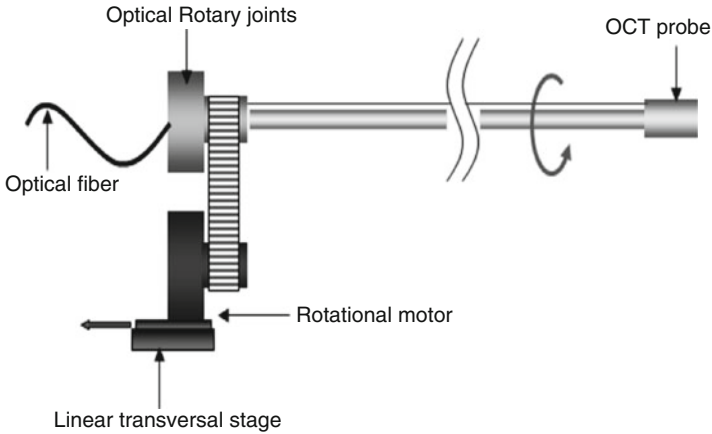
Fig. 75.3 Schematic of external rotational motor and probe

joint coupled with an externally mounted rotational motor. Torque from the motor is translated from the proximal to the distal end of the probe by a triple wound commercially available torque coil (outer diameter, 0.965 mm) (Fig. 75.3). The probe was designed to have an extended working distance of 20 mm. A Gradient Index Rod (GRIN) lens (0.23 pitch, 1-mm OD) combined with a measured spacer made of no-core fiber focuses the light from the probe. The no-core fiber was first spliced and then cleaved to leave a 150-um portion at the end of a standard single mode fiber. UV glue was used to attach fiber and GRIN lens and placed within a custom-designed metal housing. The probe is able to achieve a frame rate of 25 frames per second with each frame having 2,000 A-scans. During imaging, the probe is protected using a fluorinated ethylene propylene (FEP) sheath (OD 1.8 mm) that is first introduced into the airway. A dual motor linear stage was used for linear translation at 0.5 cm/s allowing for helical scanning over 20 cm in the span of 40 s. The axial resolution of the system was 10 μm in tissue and the lateral resolution was 112 μm, which is mainly a trade-off with extending the working distance of the probe.

Acquired OCT data is processed using a modified algorithm [21]. An FFT is first performed to convert the signal into the frequency domain. Multiplication by the Heaviside function isolates the positive frequencies, and an inverse FFT is performed to obtain a complex time-domain signal. A demodulation step removes the carrier frequency from this term and compensates the dispersion cause by the acousto-optic modulator (AOM) by multiplying the negative phase values of a single A-scan obtained when the optical path length difference (OPD) of the reference arm with the AOM and sample arm is zero. The resulting remapped data is linearized in the K-domain via a recalibration step followed by a final FFT to recover the spatial information. Our OCT software package is written entirely
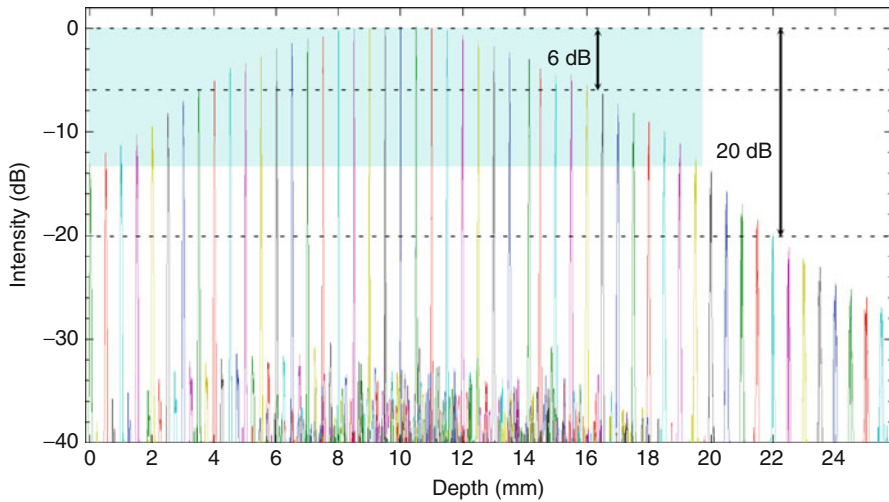
Fig. 75.4 Sensitivity of the current LR-OCT system as a function of depth

in C++ and features a multithreaded design for data acquisition, image processing, and display that allows for maximizing computational throughput. The entire OCT algorithm is processed on a commercial graphical processing unit (GPU) using Nvidia's CUDA package. This allows for frame-by-frame processing with a maximal frame rate of 25 frames per second for a given frame size of 2,000 A-lines.

75.3   Validation

The point spread function (PSF) versus imaging range graph (Fig. 75.4) was acquired by using a partial reflector at various distances and normalizing by the measured power. The system features a 6 dB sensitivity roll off at 12 mm total offset, which is in line with the expected imaging range give the removal of the mirror image.

In order to test the imaging capabilities of our system, a silicone airway was constructed. The airway was selected from a collection of adult CT scans devoid of pathology in the upper airway. The CT scan was loaded into commercial 3D rendering software, Amira, and a Standard Tessellation Language (stl) file was created for use as a model. Using rapid prototyping hardware, a phantom airway was molded in a green silicone matrix to ensure reflective properties compatible with the anatomical optical coherence tomography (aOCT) hardware (Fig. 75.4). The endoscopic LR-OCT probe and FEP sheath was introduced into the model airway in similar fashion to that of an actual research subject.

Fig. 75.5 Translucent model of normal phantom airway
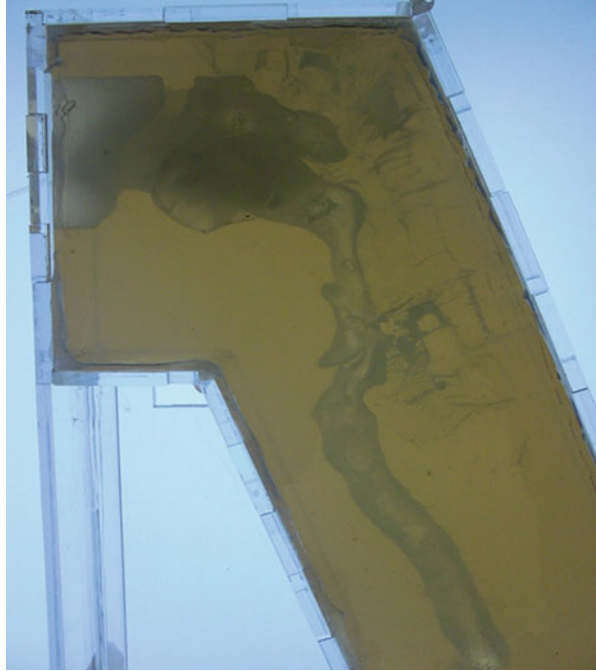
A translucent model airway (Fig. 75.5), an exact copy of the green silicone phantom, was constructed to observe the pathway of probe and FEP sheath in the upper airway. A pullback scan of the phantom airway was performed. The resulting OCT data was compared against the original CT scan. As expected, the acquired OCT images are highly correlated with the original CT scan slices (Fig. 75.6).

75.4 In Vivo Human Studies

In vivo human adult imaging has been performed on adult and pediatric subjects. Patients' upper airway was anesthetized using 4 % topical lidocaine administered bilaterally through the nostril; likewise the pharynx was anesthetized with an aerosolized benzocaine. Ten minutes was allowed to elapse in order for the anesthesia to take full effect. The subject was placed into the classical position for in-office fiber-optic endoscopy exam. The FEP sheath was inserted into the anesthetized nostril along the length of the upper airway to the level of the esophagus. FEP tubing was marked as it exited the nostril for repositioning in case movement of the pharynx shifted the probe out of position. The tubing was secured using paper tape attached to the bridge of the nose. The LR-OCT probe was
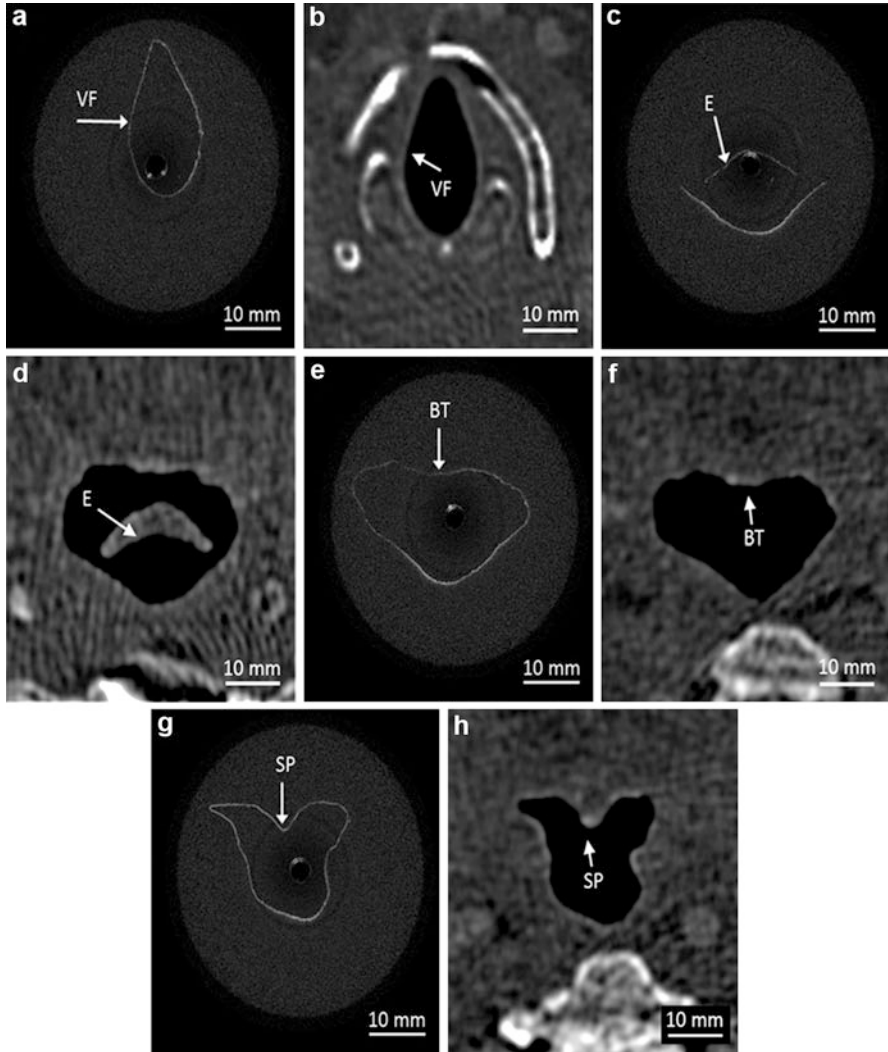
Fig. 75.6 Comparison of OCT images (**a**, **c**, **e**, **g**) in model with normal CT scan (**b**, **d**, **f**, **h**). Vocal folds (*VF*), epiglottis (*E*), base of tongue (*BT*), and soft palate (*SP*)

then advanced down the FEP tubing until resistance was appreciated (signifying the probe has reached the end of the FEP tubing). Placement of the FEP tubing and probe was confirmed using a flexible laryngoscope introduced through the second nostril, after which the laryngoscope was removed. The LR-OCT probe was retracted through the airway at a rate of 0.5 cm per second over a distance ranging from 18 to 23 cm. Multiple sets of images were taken from each subject.
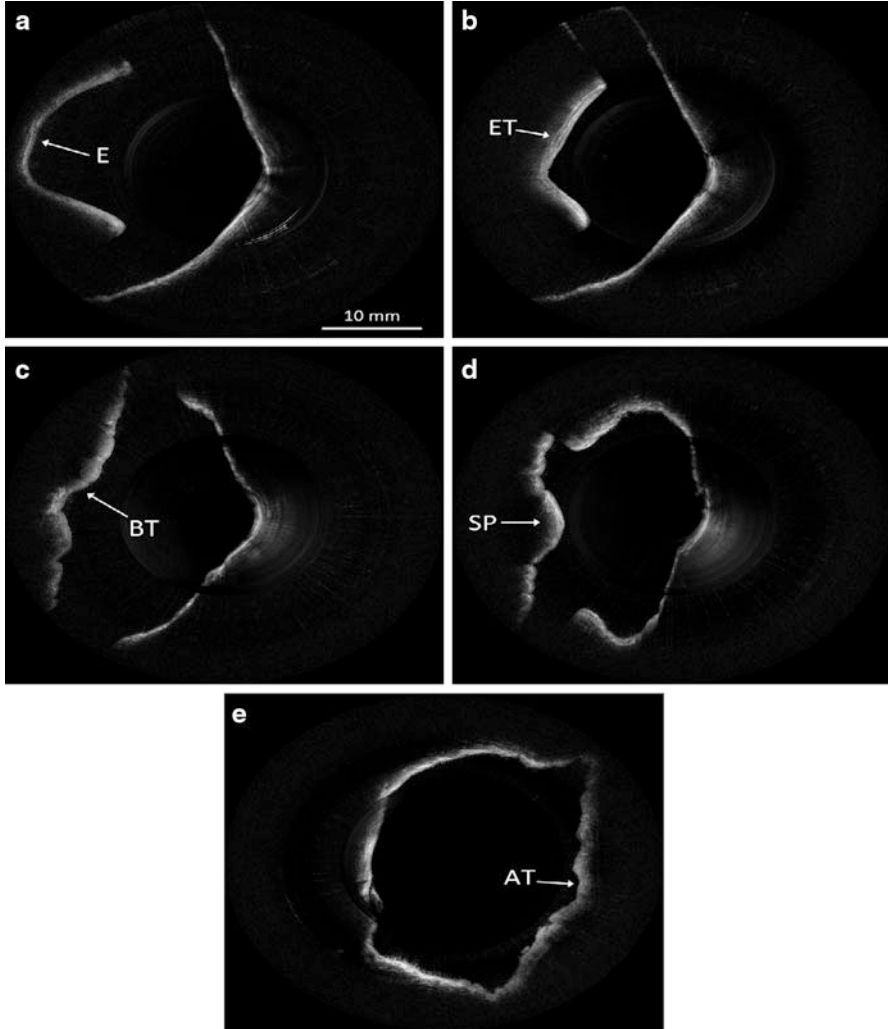
Fig. 75.7 Examples of in vivo LR-OCT images

Examples of acquired OCT data are shown in Fig. 75.7. Each cross-sectional image is 43×43 mm. Anatomical structures such as the epiglottis (Fig. 75.7a), base of tongue (Fig. 75.7b) with associated tonsillar tissue, the soft palate and uvula (Fig. 75.7c), and adenoidal tissue (Fig. 75.7d) can be identified by their distinct tissue characteristics. Unlike OCT data acquired in phantom testing, up to 1.5 mm of tissue penetration was achieved and tissue substructure such as the elastic cartilage in the epiglottis can be seen.
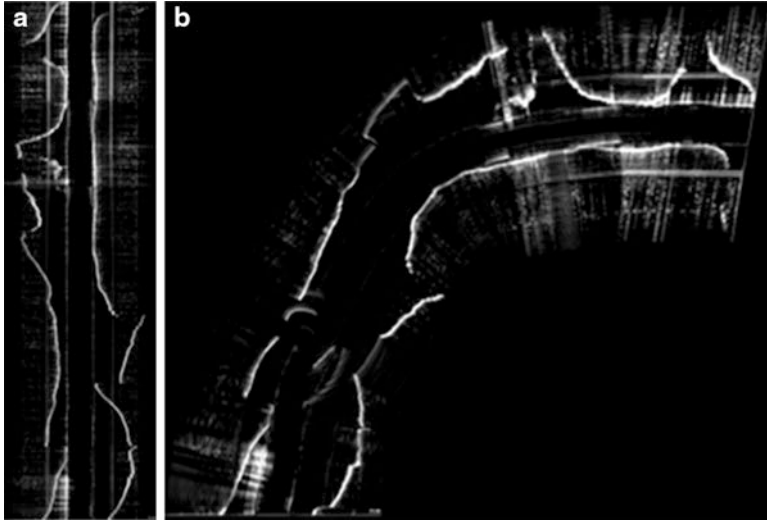
Fig 75.8 (**a**) Stacked LR-OCT data (*sagittal view*) as unprocessed linear data. (**b**) Stacked LR-OCT data (*sagittal view*) after applied bending algorithm

75.5   Image Reconstruction/Rendering

OCT images are loaded into Mimics, a commercially available 3D rendering software. Anatomically, the airway contains many bends, the most exaggerated of which occurs around the area of the soft palate and continues onto the nasal passageways. However, OCT assumes the images are acquired in a linear fashion. Unlike CT or MRI, OCT axial slices deviate from one another in an absolute coordinate system in both X-Y-Z linear displacement and at least 1 angular degree of rotations freedom. Serial OCT images must be transformed to fit along a curved airway and aligned along the "common axis." In order to fashion the linear LR-OCT data to represent the anatomical curve, a custom algorithm is used (Fig. 75.8). Using Cartesian coordinates from a series of CT scans acquired from normal patients. The database contains a variety of subjects, classified by age and sex. The acquired OCT data is matched to a CT scan that most closely correlates patient age and gender. The software creates a bend in sagittal slices of the OCT data creating an image that closely resembles the anatomic curvature. Figure 75.9 displays an example of data collection from a standard CT scan.

The literature has described an OCT probe with integrated magnetic tracking which accurately locates the tip of the OCT probe within the lumen of the airway in 3D space (X, Y, Z coordinates). This configuration can provide patient-specific airway curvatures without the need for third-party software [22]. Commercial magnetic tracking systems are now available in a small form factor (0.56 mm).

Fig. 75.9 Collection of
Cartesian coordinates from
normal CT scans for use in
custom algorithm
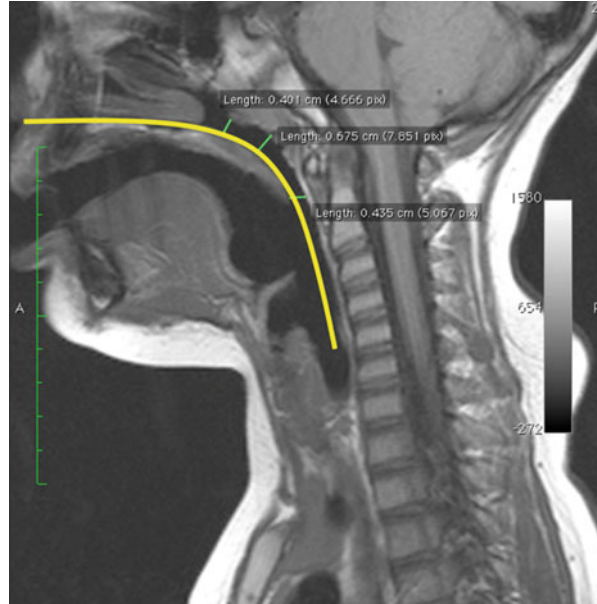
Integration with the existing LR-OCT probe has the limitation of increasing the OD
of the probe, necessitating larger outer FEP sheaths, which may lead to increased
patient discomfort. However, improvements in the technology may produce smaller
tracking beacons that will add negligible bulk to the LR-OCT probe.

After creating the bent upper airway, LR-OCT data is loaded into Mimics 3D
rendering software for construction of a volumetric model (Fig. 75.10). Using
Mimics, we are able to create accurate 3D renderings of the upper airway that will
be used in simulations to visualize flow in normal and obstructed (as in those with
OSA) airways. In Mimics, the OCT data is visualized in three planes (axial,
sagittal, and coronal). As seen in Fig. 75.7, primarily at the area of the epiglottis,
the anterior pharyngeal wall is missing. This is caused by structures (such as the
epiglottis) that cannot be penetrated by the infrared light of the LR-OCT probe.
This causes a gap in the OCT data, primarily at the level of the vallecula
and the anterior pharyngeal wall. During the creation of the volumetric rendering,
an individual equipped with endoscopic video data collected at the time of
OCT imaging must use intra-frame interpolation and knowledge of anatomy
to fill in missing data from the volume. As mentioned before, the epiglottis blocks
the area of the anterior pharyngeal wall, which manifests as a gap in the OCT
data. In order to compensate for this lack of information, the vallecula (the area
between the posterior wall of the epiglottis and the anterior pharyngeal wall)
is excluded from the reconstruction. Instead, it is assumed that the epiglottis
forms the anterior pharyngeal wall. In simulations of flow based on CT data, the
area of the vallecula does not significantly alter the flow within the airway
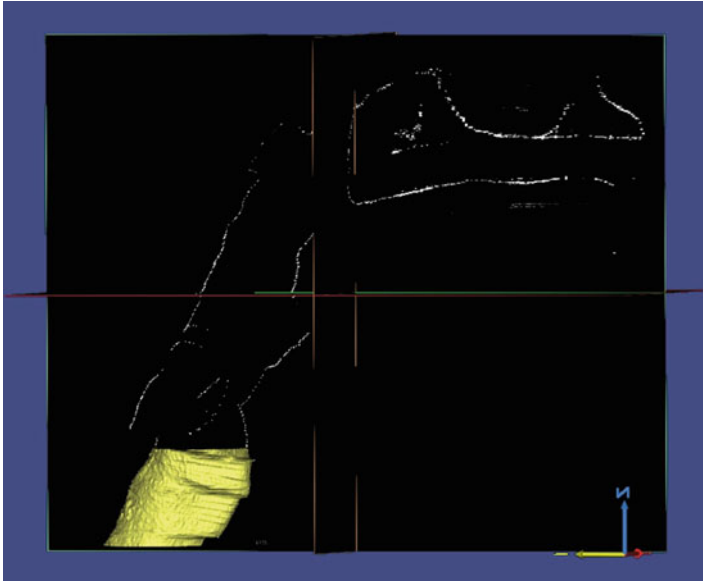(Fig. 75.11).

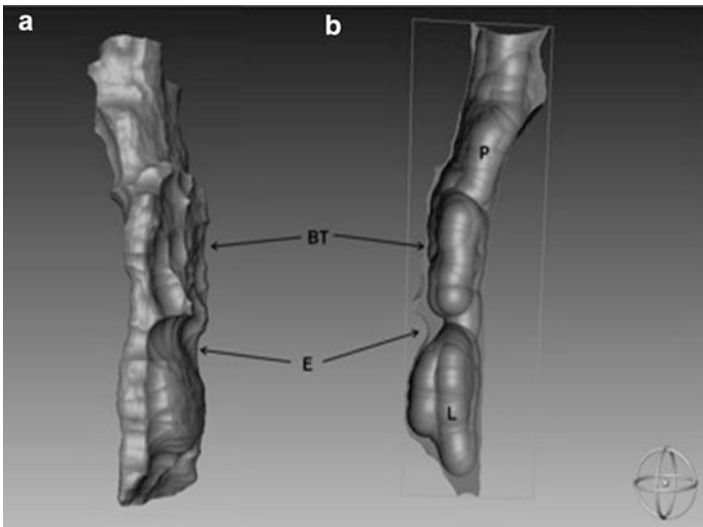**Fig. 75.10** 3D reconstruction (partial) of LR-OCT stack in Mimics™

Fig. 75.11 Completed linear 3D reconstruction of LR-OCT data. Pharynx (*P*), base of tongue (*BT*), epiglottis (*E*), and larynx (*L*)
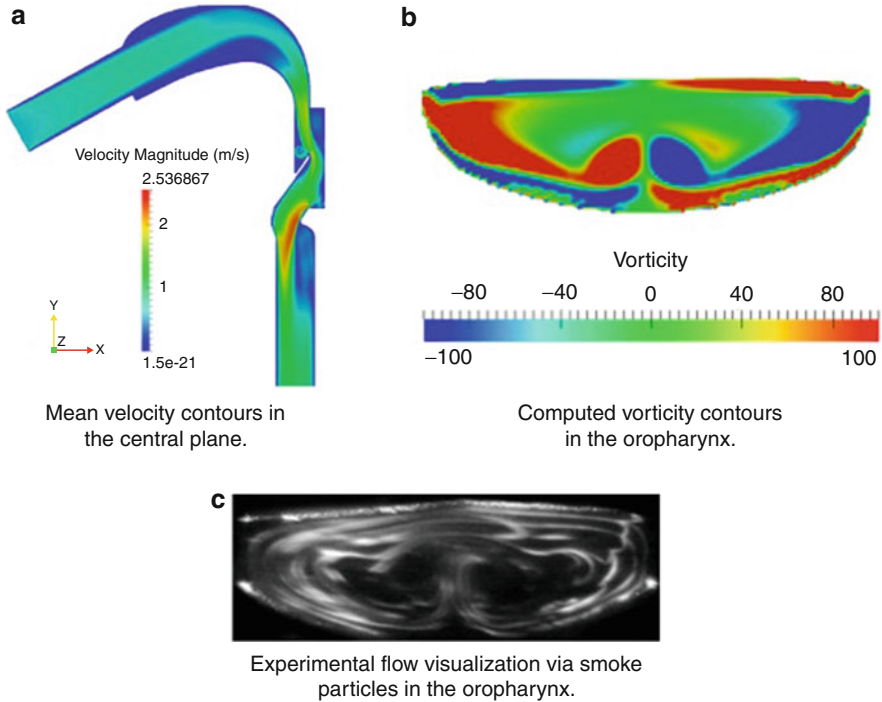
a

Velocity Magnitude (m/s)

2.536867

2

1

1.5e-21

Mean velocity contours in
the central plane.

b

Vorticity

−80   −40   0   40   80

−100   100

Computed vorticity contours
in the oropharynx.

c

Experimental flow visualization via smoke
particles in the oropharynx.

Fig. 75.12 Results of flow simulation in the idealized ETA model

75.6   Numerical Simulations and Modeling

Upper airway reconstructions created from Mimics are used to model flow using direct numerical simulation (DNS) via the lattice Boltzmann method (LBM). These flow models can be used to locate areas of possible obstruction. The simulations based on the DNS-LBM have been compared to other DNS methods for several canonical flows with similar results. Simulation of flow in an idealized ETA model geometry is presented in Fig. 75.12. Results of this simulation agree with the experimental images from the smoke array visualization.

Similar to the idealized ETA model, flow through a full upper airway reconstruction of OCT data with the bending algorithm applied (Fig. 75.13) can be visualized. Application of inlet and outlet parameters creates flow, both pressure and velocity, through the model and can be seen at various points within the upper airway (Fig. 75.14a, b).

Fig. 75.13 Full 3D reconstruction of upper airway OCT data with bending algorithm applied nasopharynx (*NP*), soft palate (*SP*), base of tongue (*BT*), and epiglottis (*E*)
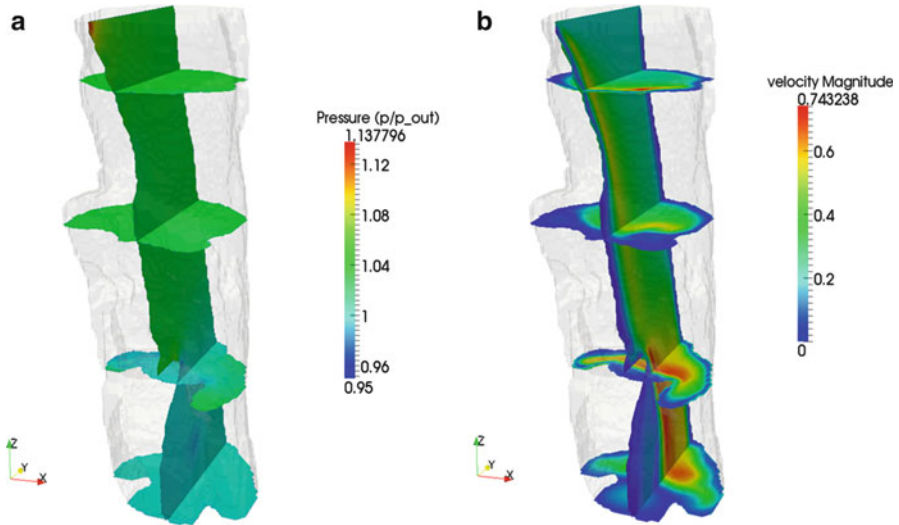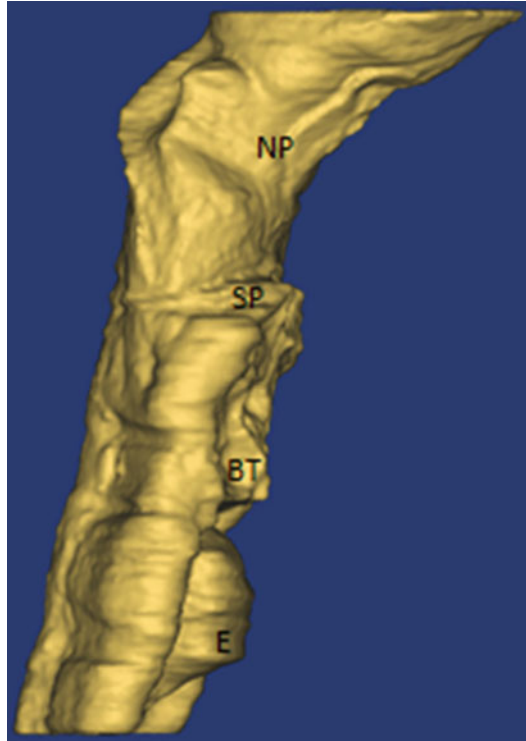

Fig. 75.14 (**a**) Pressure measurement at various levels of bent OCT data. (**b**) Air velocity measurement at various levels of bent OCT data

75.7 Conclusion

The pathophysiology of OSA is not clearly understood although it has been recognized as pathology for greater than 30 years. While polysomnography remains the standard for diagnosis, it only provides insight as to the diagnosis and does not provide anatomical detail for use in corrective surgery. Adjunct studies such as CT and MRI are not routinely used in diagnosis and management of this condition due to high cost, inconvenience, and exposure to potentially harmful radiation [23]. aOCT represents a technology that is ideally suited for use in imaging of the upper airway by being minimally invasive, easily portable, safe during extended imaging sessions, and well tolerated in awake or asleep patients [24]. The ability to simulate flow in accurate three-dimensional reconstructions can provide insight to physicians of individualized areas of obstruction. As it stands, surgical procedures for OSA are given, at best, a 50 % success rate. Localization of problem areas could lead to directed surgery and increased success rates.

aOCT is not without limitation. At certain locations within the upper airway, particularly in the hypopharynx where the epiglottis is located, more anterior tissues obstruct the imaging beam of the aOCT probe from focusing on tissues posterior to the proximal tissue. This creates gaps in axial data slices that must be manually created by correlating endoscopic images and anatomical knowledge to those particular aOCT data slices. An acquired aOCT stack is also assumed to be linear since the acquisition is recorded relative to the catheter and not in three-dimensional space. Though standardized curves extracted from age- and gender-adjusted CT scans can be applied to stacked axial OCT scans, further development of miniature magnetic tracking devices, which do not add additional bulk to aOCT probes, would allow for anatomically accurate curves to be applied to individual patient data.

aOCT has been shown to be comparative with CT for both cross-sectional area and airway structure. It can rapidly image a dynamic airway without exposure to ionizing radiation and can be used as an adjunct to polysomnography or in-office endoscopy with minimal discomfort for the patient. Time-domain systems were limited by slow scanning speeds, lower signal-to-noise ratio, and short imaging distance. Fourier-domain aOCT shows a significant scanning speed boost that is compatible with acute changes in airway structure over the breathing cycle and minimized motion artifact. An increased signal-to-noise ratio maximizes data acquisition and allows for more accurate 3D reconstructions for flow analysis.

In conclusion, imaging of upper airways with diameter of up to 3 cm was achieved in fully cognizant test subjects with minimal discomfort. Compared to an anatomical TD-OCT system, the long-range FD-OCT system not only increases the imaging speed significantly but also enhances the imaging sensitivity to enable visualization of the fine anatomical tissue structure in the airway. Combining this structural information with DNS flow simulations, we can better estimate the site and causes of airway obstruction and better select and design surgery for patients with upper airway resistance.

References

1. C. Cummings, B. Haughey, J. Thomas, *Cummings Otolaryngology: Head and Neck Surgery*, 5th edn. (Mosby, Philadelphia, 2010)

2. M. Leigh, J. Armstrong, A. Paduch, J. Walsh, D. Hillman, P. Eastwood, D. Sampson, Anatomical optical coherence tomography for long-term portable quantitative endoscopy". IEEE Trans. Biomed. Eng. **55**(4), 1438–1446 (2008)

3. Z. Abramson, S. Susarla, M. Troulis, L. Kaban, Age-related changes of the upper airway assessed by 3-dimensional computed tomography. J. Craniofac. Surg. **20**, 657–663 (2009)

4. J. Walsh, M. Leigh, A. Paduch, K. Maddison, J. Armstrong, D. Sampson, D. Hillman, P. Eastwood, Effect of body posture on pharyngeal shape and size in adults with and without obstructive sleep apnea". Sleep **31**(11), 1543–1549 (2008)

5. J. Armstrong, M. Leigh, I. Walton, A. Zvyagin, S. Alexandrov, S. Schwer, D. Sampson, In vivo size and shape measurement of the human upper airway using endoscopic long- range optical coherence tomography. Opt. Express **11**(15), 1817–1826 (2003)

6. G. Tearney, M. Brezinski, J. Southern, B. Bouma, S. Boppart, J. Fujimoto, Optical biopsy in human urologic tissue using optical coherence tomography. J. Urol. **157**, 1915–1919 (1997)

7. J. Izzat, M. Kulkarni, H. Wang, K. Kobayashi, M. Sivak, Optical coherence tomography and microscopy in gastrointestinal tissues. IEEE J. Sel. Top. Quant. Electron. **2**(4), 1017–1028 (1996)

8. J. Williamson, R. McLauglin, W. Noffsinger, A. James, V. Baker, A. Curatolo, J. Armstrong, A. Regli, K. Shepard, G. Marks, D. Sampson, D. Hillman, P. Eastwood, Elastic properties of the central airways in obstructive lung diseases measured using anatomical optical coherence tomography. Am. J. Respir. Crit. Care Med. **183**, 612–619 (2011)

9. R. McLaughlin, J. Armstrong, S. Becker, J. Walsh, A. Jain, D. Hillman, P. Eastwood, D. Sampson, Respiratory gating of anatomical optical coherence tomography images of the human airway. Opt. Express **17**(8), 6568–6577 (2009)

10. J. Williamson, R. McLaughlin, M. Phillips, J. Armstrong, S. Becker, J. Walsh, D. Sampson, D. Hillman, P. Eastwood, Using optical coherence tomography to improve diagnostic and therapeutic bronchoscopy. Chest **136**(1), 272–276 (2009)

11. P. Williamson, A. James, M. Phillips, D. Sampson, D. Hillman, P. Eastwood, Quantifying dimensions of the tracheobronchial tree: methods, limitations and emerging techniques. Eur. Respir. J. **34**(1), 42–55 (2009)

12. J. Williamson, J. Armstrong, R. McLaughlin, P. Noble, A. West, S. Becker, A. Curatolo, W. Noffsinger, H. Mitchell, M. Phillips, D. Sampson, D. Hillman, P. Eastwood, Measuring airway dimensions during bronchoscopy using anatomical optical coherence tomography. Eur. Respir. J. **35**(1), 34–41 (2010)

13. J. Walsh, M. Leigh, A. Paduch, K. Maddison, D. Philippe, J. Armstrong, D. Sampson, D. Hillman, P. Eastwood, Evaluation of pharyngeal shape and size using anatomical optical coherence tomography in individuals with and without obstructive sleep apnea. J. Sleep Res. **17**, 230–238 (2008)

14. R. Leitgeb, C. Hitzenberger, A. Fercher, Phase-shifting algorithm to achieve high-speed long-depth-range probing by frequency-domain optical coherence tomography. Opt. Lett. **28**(22), 2201–2203 (2003)

15. J. Armstrong, M. Leigh, D. Sampson, J. Walsh, D. Hillman, P. Eastwood, Quantitative upper airway imaging with anatomic optical coherence tomography. Am. J. Respir. Crit. Care Med. **173**, 226–233 (2006)

16. S. Huang, A. Aguirre, R. Huber, D. Adler, J. Fujimoto, Swept source optical coherence microscopy using a Fourier domain mode-locked laser. Opt. Express **15**(10), 6210–6217 (2007)

17. A. Fercher, W. Drexler, C. Hitzenberger, T. Laser, Optical coherence tomography- principles and applications. Rep. Prog. Phys. **66**, 239–303 (2003)

18. A. Fercher, C. Hitzenberger, G. Kamp, S. El-Zaiat, Measurement of intraocular distances by backscattering spectral interferometry. Opt. Commun. **117**, 43–48 (1995)
19. A. Lucey, A. King, G. Tetlow, J. Wang, J. Armstrong, M. Leigh, A. Paduch, J. Walsh, D. Sampson, P. Eastwood, D. Hillman, Measurement, reconstruction, and flow-field computation of the human pharynx with application to sleep apnea. Trans. Biomed. Eng. **57**(10), 2535–2548 (2010)
20. R. Huber, M. Wojtkowski, J. Fujimoto, Fourier Domain Mode Locking (FDML): a new laser operating regime and applications for optical coherence tomography. Opt. Express **14**(8), 3225–3237 (2006)
21. J. Zhang, J. Nelson, Z. Chen, Removal of a mirror image and enhancement of the signal-to-noise ration in Fourier-domain optical coherence tomography by use of an electro-optical phase modulator. Opt. Lett. **30**(2), 147–149 (2005)
22. B. Lau, R. McLaughlin, A. Curatolo, R. Kirk, D. Gerstmann, D. Sampson, Imaging true 3D endoscopic anatomy by incorporating magnetic tracking with optical coherence tomography: proof-of-principle for airways. Opt. Express **18**(26), 27173–27180 (2010)
23. S.P. Patil, H. Schneider, A.R. Schwartz, P.L. Smith, Adult obstructive sleep apnea: pathophysiology and diagnosis. Chest **132**(1), 325–337 (2007)
24. J. Armstrong, M. Leigh, J. Walsh, D. Hillman, P. Eastwood, D. Sampson, Anatomical optical coherence tomography for imaging the human upper airway. In: W. Drexler, J.G. Fujimoto (eds), *Optical Coherence Tomography. Biological and Medical Physics, Biomedical Engineering* (2008), Springer Berlin Heidelberg, pp. 1269–1292